Chapter 4
Critical Current Anisotropy in Relation to the Pinning Landscape

Nick J. Long

4.1 Introduction

Raising the critical currents of high-temperature superconductors has the desirable outcome of lowering the barrier to widespread application of these materials. With creative materials engineering, researchers have been successful in improving critical currents over the field and temperature ranges relevant to applications [1–7]. Intrinsic thermodynamic properties and the interaction between the magnetic vortices and the pinning landscape combine to determine how much current is supported. Due to both factors, the resultant critical currents generally vary with the angle of the imposed external field. In this chapter, we will explore what is known about this anisotropy.

The key to improved critical current performance has been optimizing the density and morphology of pinning centers both for native crystal defects, such as ion vacancies, stacking faults, and dislocations, and engineered additions such as randomly distributed normal phase nanoparticles, columnar and transverse arrays of nanoparticles. The improvements made in critical currents have been achieved by trial and error guided by the understanding that it is desirable to have pinning centers which are of similar dimension to the superconductor coherence length, and that defects which are correlated in one direction will mostly enhance pinning when the external magnetic field is also oriented in this direction. To go beyond trial and error and more rationally improve nanoengineering of the pinning landscape, we need to better understand the structure-property relationships between the pinning microstructure and the critical current density.

But analyzing the critical current density to produce structure-property relationships has not proved straightforward or without controversy for the anisotropic

N.J. Long (✉)
Robinson Research Institute, Victoria University of Wellington,
Wellington, New Zealand
e-mail: Nick.Long@vuw.ac.nz

superconductors. The difficulty stems partially from having two sources of aniso-tropy, the anisotropy in the vortex cross section, arising from the intrinsic mass anisotropy of the carriers of the vortex current, and the anisotropy of the pinning centers themselves. The effects of these two factors are not easily separated. It is never possible to have a fully isotropic pinning landscape in an anisotropic superconductor. By definition, the modulation of the superconductor order parameter in the *c*-axis direction gives some directional pinning. In addition, par-ticularly for thin films, some correlated native defects in the *c*-axis or *a/b* axis directions are inevitable. The other aspect of the difficulty lies in data analysis, as we will describe in this chapter these two effects can produce similar outcomes.

A better understanding of the structure-property relations has technical value as the anisotropy in critical currents complicates the use of these superconductors. In most applications, wires and tapes will experience magnetic fields at many different angles to the tape. If the critical current (I_c) varies strongly with angle, this presents challenges for coil designers who must keep the coil within safe operating margins of I/I_c everywhere within the coil. An unpredictable or only weakly predictable I_c with field and temperature means exploiting the full capacity of these materials is compromised.

Scientifically, the anisotropy of $I_c(\theta)$ highlights that for anisotropic supercon-ductors or even superconductors in general, we do not understand well enough the structure-property relationships between pinning and critical currents. The phe-nomenon of pinning is not in dispute, but the understanding of how pinning is aggregated across a complex pinning landscape, and the role played by carrier anisotropy, is not complete.

Therefore, in this chapter, we will look at the common methods used to extract information about the pinning landscape and the role of mass anisotropy from measurements of the critical current density anisotropy $J_c(\theta)$. We define $J_c = I_c/A$ as the critical current density in the plane of the tape or thin film, or *ab*-plane in the case of a crystal, and θ is the angle between the applied magnetic field and the normal to the tape, usually the *c*-axis direction, with the current always perpen-dicular to the field. This is often referred to as the maximum Lorentz force con-figuration and is of most relevance to magnet and coil design.

Experimentally, we define the transport critical current as the current when an electric field $E_0 = 1$ µV/cm is present in the current direction. The $E(J)$ relation for transport currents is found to be a power law $E/E_0 = (J/J_c)^n$ so strictly we have an arbitrary engineering criterion rather than a value uniquely determined by experi-ment. With magnetization measurements of J_c, the electric field criterion is effec-tively much lower although this does not affect the analyses examined here. Theoretically, the critical current is defined by $\vec{J}_c \times \vec{\Phi}_0 + \vec{p}_{max} = 0$ [8, 9], that is, the sum of the forces on the vortex arising from the presence of the transport current is in balance with the restoring force on the vortex due to its spatial position in a potential minimum. Researchers commonly call the force due to the current the Lorentz force although there are good reasons not to do this [9, 10]. We shall persist with the mainstream nomenclature and refer to this as the Lorentz force.

Common methods to analyze the critical current anisotropy are firstly scaling methods, such as the Blatter scaling [8, 11] and other scaling approaches which are a modification of this approach. Secondly, there are more direct methods of calculating the expected response from defects, which examine the pinning forces on vortices from defects under certain assumptions, and finally, we examine the vortex path model or maximum entropy method, which is an information theory or statistical approach for extracting information from $J_c(\theta)$.

4.2 Mass Anisotropy Scaling

4.2.1 Theory

For high-temperature superconductors, taking account of the fundamental electronic anisotropy of the materials is necessary to understand the thermodynamic and electromagnetic properties. Hao and Clem [12] first discussed how the Gibbs free-energy difference ΔG between the mixed and normal states can be expressed as a function of the reduced field $h(\theta) = \frac{H}{H_{c2}(\theta)} \propto H\epsilon(\theta)$ for $H \gg H_{c1}$, where $\epsilon(\theta) = (cos^2\theta + \gamma^{-2}sin^2\theta)^{1/2}$ and $\gamma = \sqrt{m_c/m_{ab}}$ is the mass anisotropy parameter. They hypothesized that physical quantities derived from the Gibbs free energy should obey the same scaling behavior. Hence, measurements of these properties should be scalable with the magnetic field in the same way through the reduced field h. These properties would include resistivity, critical current density, and flux-line-lattice melting temperature. They thus proposed the scaling $J_c(H, \theta) = J_c(h(\theta))$ for the critical current.

Blatter et al. [8, 11] expanded on and generalized this idea by noting that the conventional method for accommodating anisotropy into a phenomenological model of superconductivity is to introduce an anisotropic effective mass tensor into the Ginzburg–Landau or London equations and then proceed to repeat calculations made for the isotropic case. Instead, they proposed to rescale the anisotropic problem to a corresponding isotropic one at the level of the basic phenomenological equations. The scaling rules can then be applied to the known results of the isotropic model to obtain the anisotropic results with no great effort. This approach is schematically represented in Fig. 4.1.

The primary result is then a scaling rule as given in (4.1), where the desired quantity is Q and the known isotropic result is $\widetilde{Q}$.

$$Q(\theta, H, T, \xi, \lambda, \varepsilon, \gamma_B) = s_Q \widetilde{Q}(\epsilon_\theta H, T/\varepsilon, \xi, \lambda, \gamma_B/\varepsilon) \qquad (4.1)$$

Blatter et al. use different conventions from those now typical in critical current research, so in (4.1), ε is the reciprocal of our anisotropy factor, i.e., $\gamma = 1/\varepsilon = 5 - 7$ for YBCO and γ_B is not anisotropy but is a measure of the disorder. Blatter et al. derived these results in the context of weak collective pinning theory, where γ_B
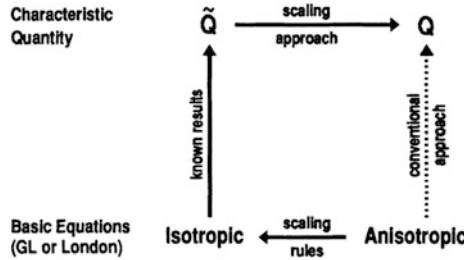
Fig. 4.1 Scaling procedure to simplify the derivation of anisotropic models as proposed by Blatter et al. There are two paths to go from the basic equations of superconductivity to a model of the measured quantity Q, either via a direct calculation or via scaling rules, which transform the basic equations from anisotropic to isotropic. (Figure reproduced from [11] with permission)

describes short-range disorder in T_c. This scaling rule leads Blatter et al. to also predict for the planar critical currents in an anisotropic superconductor $J_c(H, \theta) = J_c(h(\theta))$, for large magnetic fields, consistent with Hao and Clem [12]. At low fields in the single vortex regime, a direct substitution of the scaling rules in the collective pinning theory gives a different result, $J_c(\theta) = \text{const}$, [8].

4.2.2 $J_c(h(\theta))$ Scaling of YBCO

The $J_c(H, \theta) = J_c(\epsilon_\theta H)$ scaling law was first applied to the critical currents in YBCO films by Xu et al. [13] and Kumar et al. [14]. For Xu et al., the scaling relationship worked reasonably well over the whole angular range, over a wide field range at high temperature. They plotted their data in the form of flux pinning force or 'Kramer scaling' with a driving force of $F_p^{eff} = J_c \epsilon_\theta H = F_0 h(\theta)^p (1 - h(\theta))^q$ and found a single scaling curve for F_p^{eff} versus h with no further rescaling of F_p. This is equivalent to finding a single curve for $J_c(\epsilon_\theta H)$ versus h as in the experiments described over the next few paragraphs. Xu et al., who referenced Hao and Clem, did not argue that the scaling implied any particular type of pinning structure, rather they argued from the exponents of the Kramer scaling that planar pinning mechanisms were dominant with some point pinning. Kumar et al. referenced [8] and did not discuss pinning mechanisms; they found $\gamma = 3.4$ gave the best overlap of data.

The technique was not applied more commonly until Civale et al. used it to identify the effect of particular pinning structures [15, 16]. Civale et al. argued that the $J_c(\epsilon_\theta H)$ scaling would apply to *random defects* (uncorrelated disorder) only, and hence by identifying the component of critical current which followed the scaling rule, the components which corresponded to correlated defects could be separately identified. Figure 4.2 shows the process applied to make this assignment given a set of $J_c(\theta)$ curves at various values of H. Firstly, the $J_c(\theta)$ is replotted as $J_c(\epsilon_\theta H)$ with γ as the only adjustable parameter. The procedure is repeated with

every dataset for different H. If the correct value of γ is chosen, then the data collapse onto a single curve, except for the regions where correlated pinning is contributing to J_c. A single curve can then be fitted to $J_c(\epsilon_\theta H)$ which covers the region of overlapping data. This fitting can then be mapped back to any single dataset $J_c(\theta)$ to identify the portion of the curve attributable to random pinning, and this contribution subtracted to quantitatively identify the correlated pinning. The result shown in Fig. 4.2 is typical for many YBCO films which have correlated pinning due to *ab*-plane pinning centers, either intrinsic pinning from the weakly superconducting spacing layers or stacking faults, and *c*-axis pinning due to either grain boundaries or twin plane boundaries.

This method can then be applied to investigate the temperature and field dependence of particular pinning contributions. This was done in detail by Gutierrez et al. [2] for a metal-organic deposited YBCO film with barium zirconate (BZO) inclusions.
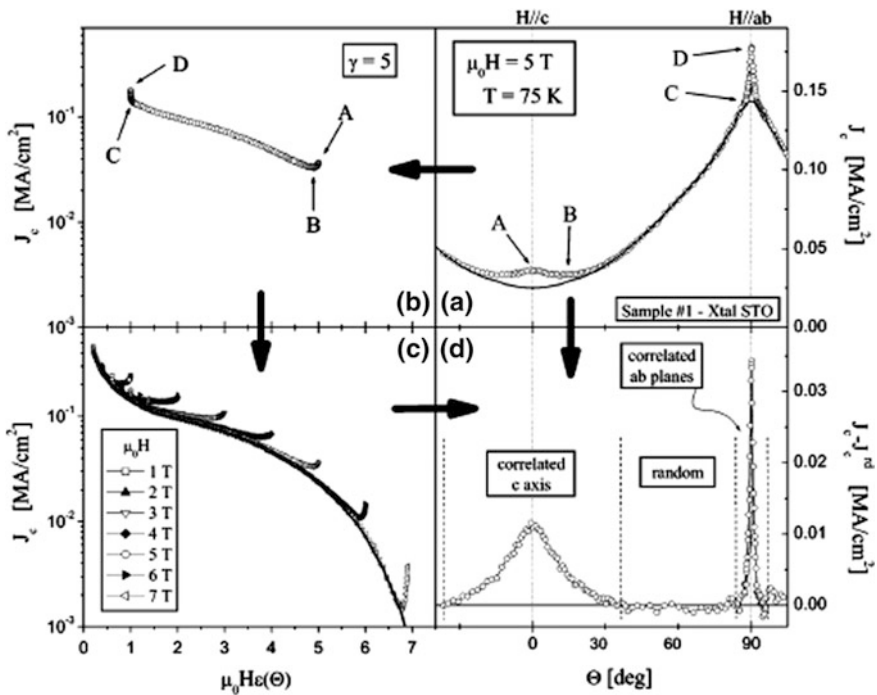

Fig. 4.2 Application of the scaling method to separate isotropic and anisotropic components. **a** $J_c(\theta)$ for an YBCO film at B = 5 T, the solid line is the identified isotropic contribution to $J_c(\theta)$ from the scaling approach, **b** A scaled $J_c(h(\theta))$ dataset, where A, B, C, D are data points for $\theta = 0$, 15, 85, 90°, respectively. **c** scaled data for the full set of fields, the solid line is a fit to where the data overlap and is identified as the random isotropic contribution to J_c **d** anisotropic contributions to $J_c(\theta)$ at 5 T obtained by subtracting the isotropic $J_c(\theta)$. (Figure reproduced from [15] with permission)

This paper reported the largest flux pinning forces in an HTS or LTS conductor to that date, a value of ~21 GN m^{-3} at 77 K, and ~80 GN m^{-3} at 65 K. This was an impressive 500% improvement over NbTi at 4 K.

The film incorporated a dense array of mostly randomly oriented BZO nanodots, i.e., embedded particles of ~15 − 30 nm diameter at a concentration of 10% mol. The film was also dense with further defects such as stacking faults (single Y-124 layers) and intergrowths (blocks of YCuO$_x$ or BaCuO$_x$). XRD analysis of the films showed them to have an internal strain of 0.56%, which was twice that of pure YBCO films prepared with the same technique.

The effect of these different pinning structures was resolved through the technique of Fig. 4.2, collapsing the $J_c(H, \theta)$ curves onto a single-scaled $J_c(\epsilon_\theta H)$. To achieve an overlap of the data required setting $\gamma_{eff} \sim 1.5$ compared to the usual $\gamma \sim 5 - 7$ for YBCO, that is, the effective anisotropy of this material is much lower than pure YBCO. The authors then went a step further by assuming critical currents due to weak collective pinning can be described by a temperature dependence $J_c^{wk}(T) = J_c^{wk}(0)\exp(-T/T_0)$ and those due to strong pinning can be described by $J_c^{str}(T) = J_c^{str}(0)\exp[-3(T/T^*)^2]$. The contributions to J_c can thus be further decomposed by fitting the isotropic $J_c^{iso}(T)$ or anisotropic $J_c^{anis}(T)$ with a mixture of these expressions. Their results are shown in Fig. 4.3 for a range of temperatures and fields. Figure 4.3a shows for H//c the isotropic contribution is dominant at all fields. Figure 4.3b shows the full temperature dependence of the isotropic J_c and that this can be fitted using the strong pinning model at high fields and a combination of weak and strong at 1 T. The final plot, Fig. 4.3c, shows how the complete $J_c(T)$ can be decomposed into weak and strong pinning components if we ignore the small anisotropic contribution for H//c. This can be generalized to a pinning phase diagram showing how strong pinning is dominant for higher fields and temperatures, and weak pinning becomes significant only at temperatures < 15 K.

Following on from this work, the same authors and others have used $J_c(\epsilon_\theta H)$ scaling to quantify the effects of nanostructuring on critical currents. Also using metal-organic deposition (MOD) as the fabrication technique, self-assembled nanowires of Ce$_{0.9}$Gd$_{0.1}$O$_{2-y}$ (CGO) or nanoislands of (La,Sr)O$_x$ can be prepared on single crystal substrates, [17]. Both surface modifications are shown to induce extended c-axis defects leading to an increase in critical currents for H//c. Using the $J_c(\epsilon_\theta H)$ scaling, the ratio of anisotropic pinning to total current over the (H, T) region is shown in Fig. 4.4 for the sample with LSO nanodots. Of note is the weak field dependence of the pinning. It appears the added c-axis pinning is quite effective to high fields, and is most effective at high temperatures. This is borne out by a direct comparison of the pinning engineered films with a pure YBCO reference film [17].

An important follow-up to this work was the investigation on the effects of strain in the MOD films [18]. It was found that nanocomposites of YBCO-BaZrO$_3$ and YBCO-Ba$_2$YTaO$_6$ enhanced the generation of strain—correlated with the interfacial area of the nanodots. The strain itself is of such a magnitude as to suppress pair formation and hence can be a source of vortex pinning. Through comparisons with
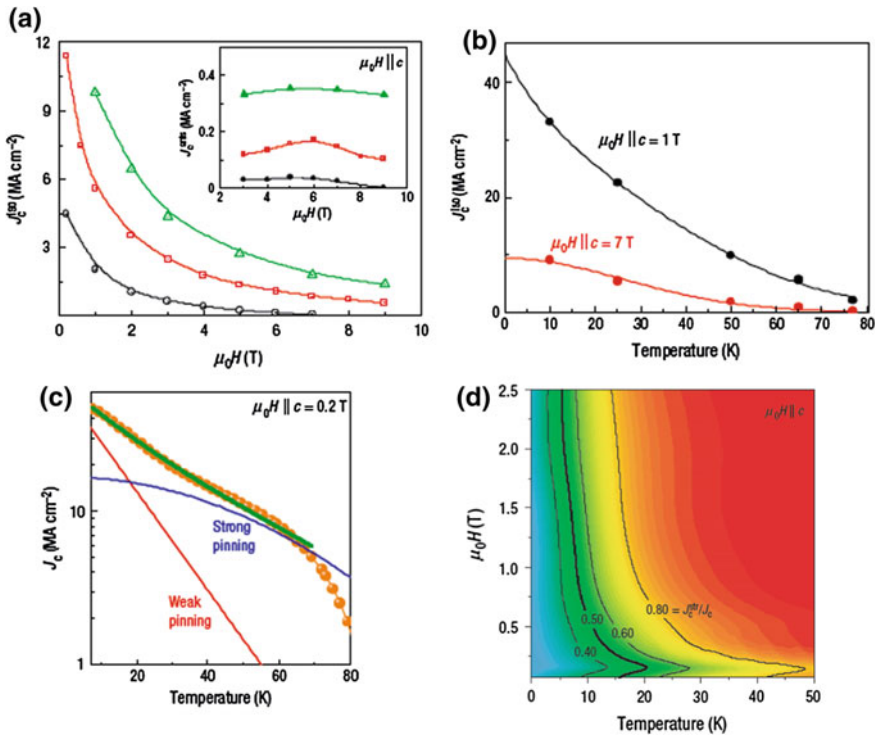
Fig. 4.3 Separation of isotropic/anisotropic and weak/strong components of the critical current. **a** Field dependence $J_c^{iso}(B)$ and $J_c^{anis}(B)$ at different temperatures, **b** temperature dependence $J_c^{iso}(T)$ at two fields. 7 T data are fitted to the strong pinning expression, and 1 T data are fitted to a mixed weak-strong expression. **c** J_c measured inductively (effectively the isotropic critical current only) and a fit of the weak and strong contributions. **d** Pinning phase diagram showing the contribution of strong pinning to the total critical current for H//c, as deduced from the fitting of **c**. (Reproduced from [2] with permission.)

Fig. 4.4 Vortex pinning phase diagram showing the ratio of anisotropic to total critical current J_c^{anis}/J_c for H//c over a range of field and temperature for a YBCO sample prepared on a substrate with a surface preparation of LSO nanoislands. (Reprinted from Gutiérrez et al. [17] with permission)
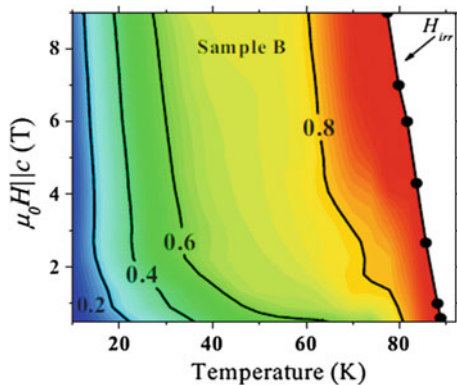
different nanoparticle additions, they identify strain as a source of increased iso-
tropic pinning force. These samples also have high densities of Y124 stacking
faults. The result is samples with a low effective anisotropy of $\gamma_{eff} \sim 1.4$, compared
to the confirmed mass anisotropy from $H_{c2}(\theta)$ of $\gamma \sim 5.9 - 6$ [18].

Despite the success of these approaches in assessing the effects of nanostruc-
turing, we may harbor some reservations about the assignment of these components
vis-a-vis weak/strong and isotropic/anisotropic pinning. The weak collective pin-
ning theory on which Blatter et al. derived their formulation has an expression for
critical current of $J_c \approx J_0[\xi/L_c]^2$ and only applies when the collective pinning
length is much larger than the coherence length, $L_c \gg \xi$ [8]. For REBCO films
which have critical currents on order of 10% of J_0, we would have a collective
pinning length $L_c \sim \xi$. This is an inconsistency—high-performance REBCO films
are not in the weak collective pinning limit. The use of anisotropy factors which are
substantially different from the electronic mass anisotropy also invites questions as
to what exactly this parameter represents. As confirmed by the authors themselves,
the intrinsic electronic mass anisotropy has not changed. To explore these issues
further we will take a brief look at similar scaling for other materials.

4.2.3 $J_c(h(\theta))$ Scaling of BSCCO

A scaling description can also be used on BSCCO $(Bi, Pb)_2Sr_2Ca_2Cu_3O_{11}$ wires as
shown in Fig. 4.5 [19]. BSCCO is known to have a very complicated
microstructure, so that a combination of *ab*-plane defects and point defects will
exist. The material is also poorly textured compared with the YBCO thin films
discussed thus far, and will have a FWHM of the rocking curve of order 12° [20]. In
this plot, data for temperatures from 20–85 K have been combined by scaling the I_c
to the self-field value at each temperature. This data can be fitted with a
(temperature-independent) anisotropy parameter, $\gamma \approx 8$, which is similar to results
from YBCO, although this bears no relation to the real mass anisotropy of the
material, which is conservatively estimated at $\gamma \approx 50$. [8, 21]

This general ability of $J_c(\epsilon_\theta H)$ to produce a convenient parameterization of large
datasets has been exploited by Hilton et al. [22] and Pardo et al. [23] who have used the
mass anisotropy expression to fit datasets of YBCO over wide ranges of temperature
and field, for samples with I_c maxima at perpendicular and/or parallel fields.

It is not clear exactly why this parameterization works so well. One reason is
undoubtedly that $J_c(\epsilon_\theta H) \approx J_c(H\cos\theta)$ over much of the angular range, and this is
insensitive to the γ value. Hence, if critical current is proportional to the flux density
perpendicular to the layers, where the pinning may be less strong, then this fitting
will work reasonably well. It is only close to parallel field that the γ value has a
strong effect, but if the fitting is poor closer to parallel field, it is easy to invoke
correlated pinning as the reason. We should therefore be sensitive to the possibility
of misinterpretation using this technique.

Fig. 4.5 Scaling of BSCCO wire for temperatures of $20 - 85$ K, and fields up to 8 T. The field was scaled using $\epsilon(\theta)B/B_{irr}$ with $\gamma = 8$. The B_{irr} values used are shown in the inset. The critical currents are normalized to the self-field value at each temperature. Reprinted from [19] with permission
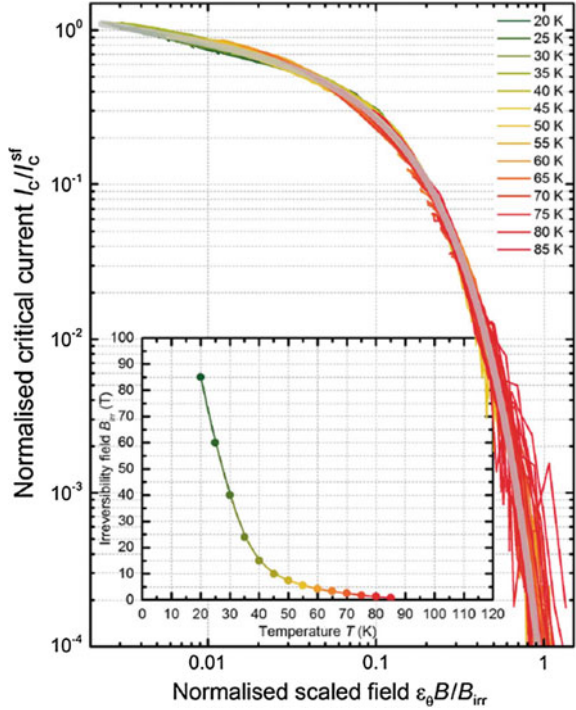
4.2.4 $F_p(h(\theta))$ Scaling of Ba-122

An interesting experimental exploration of the validity of scaling rules has recently been published by Mishev et al. [24]. They have studied $J_c(\theta)$ in $BaFe_2As_2$ (Ba-122)-based superconducting single crystals, with three samples covering weak, intermediate, and strong pinning regimes. Starting with a K-doped Ba-122 crystal with the lowest J_c, this sample was shown to obey $J_c(\epsilon_\theta H)$ scaling. For an example of strong pinning, they prepared a neutron-irradiated Co-doped Ba-122 sample, with isotropic defects which are larger than the coherence lengths. For this sample, $J_c(\epsilon_\theta H)$ scaling does not produce a collapsed curve, instead they found that an additional scaling factor is required $J_c(H, \theta) = \epsilon_\theta J_c(\epsilon_\theta H)$ which then produces a single curve for the data. As this is equivalent to scaling the flux pinning force, i.e., $J_c(H, \theta)\mu_0 H = \mu_0 \epsilon_\theta H J_c(\epsilon_\theta H)$ or in the common Kramer form $F_p(H, \theta) = F_0 h(\theta)^m (1 - h(\theta))^n$, we will refer to this as $F_p(\epsilon_\theta H)$ or $F_p(h(\theta))$ scaling. Mishev et al. motivate this scaling using an argument associated with Fig. 4.6 below.

Mishev et al. argue that the elementary pinning force, $f_p = E_p/d$, where E_p is the pinning energy and d is the relevant length scale, is for defects with a radius less than the coherence length, $r_d < \xi_{ab}$, $f_p \propto E_c r_d^3/\xi_{ab}\epsilon(\theta)$, with E_c the condensation energy, which retains an angular dependence. This is illustrated in Fig. 4.6e, f. In contrast, for a large defect with $r_d \geq \xi_{ab}$, $f_p \propto E_c r_d \xi_{ab}\epsilon(\theta)/\epsilon(\theta) = \text{const}$. This is
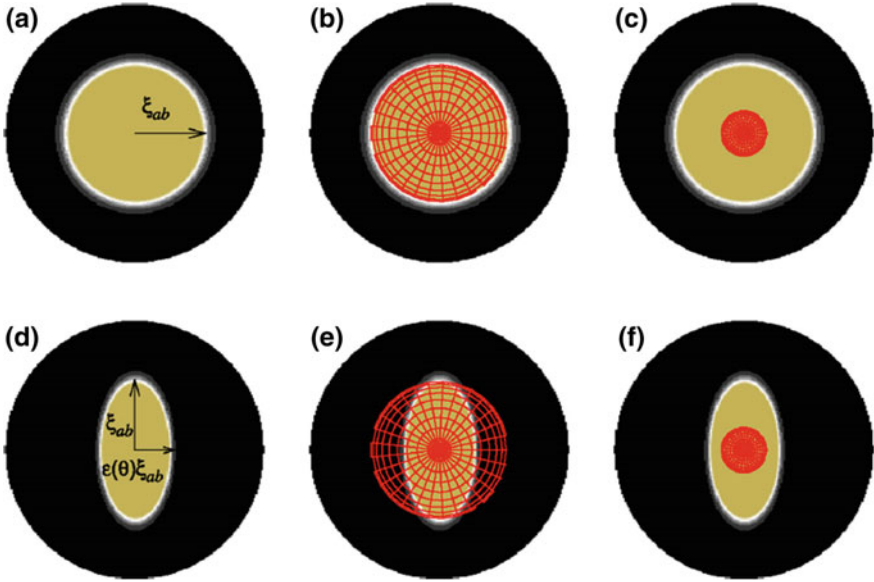
Fig. 4.6 Figure from Mishev [24] giving a microscopic explanation as to why critical currents arising from larger defects would produce a different scaling rule from those arising from point defects **a** isotropic vortex core **b** isotropic core pinned by large defect, $r_d \geq \xi_{ab}$ **c** core pinning by small defect, $r_d < \xi_{ab}$, **d** the vortex core after a rotation by angle θ **e** pinning of the anisotropic core by a large defect, **f** pinning of the anisotropic core by a small defect. Reprinted from [24] with permission

illustrated in Fig. 4.6b, e. This fundamental difference in the elementary pinning force produces the difference in scaling of the macroscopic currents, that is, between $J_c(\epsilon_\theta H)$ scaling and $F_p(\epsilon_\theta H)$ scaling.

This argument introduces some additional puzzles, however. If for the case of $r_d \geq \xi_{ab}$, the elementary pinning is angle independent, and these defects are dominant, then how physically does the angular dependence of the critical currents arise? From our definition of the critical current, $\overrightarrow{J}_c \times \overrightarrow{\Phi}_0 + \vec{p}_{max} = 0$, the angular dependence in J_c must arise from pinning interactions of some description.

This $F_p(\epsilon_\theta H)$ scaling has been proposed previous to the Mishev et al. paper to describe critical currents in an irradiated YBCO sample. Matsui et al. [25] prepared YBCO films with an MOD method and then applied low-energy Au irradiation to produce a large density of point like pins. Matsui et al. noticed that if they transform their J_c data for the irradiated film into flux pinning force, the result is an interesting 'capping' of the magnitude of the flux pinning force, seemingly independent of field. This is shown in Fig. 4.8d. In an inset of Fig. 4.8c are calculated values of $F_p(H, \theta) = F_0 h(\theta)^m (1 - h(\theta))^n$, with $(m, n) = (0.5, 2)$, and the scaling used is $h(\theta) = \epsilon(\theta)H/H_0$ with $\mu_0 H_0 = 8.3$ T. This function is shown to fit the data in
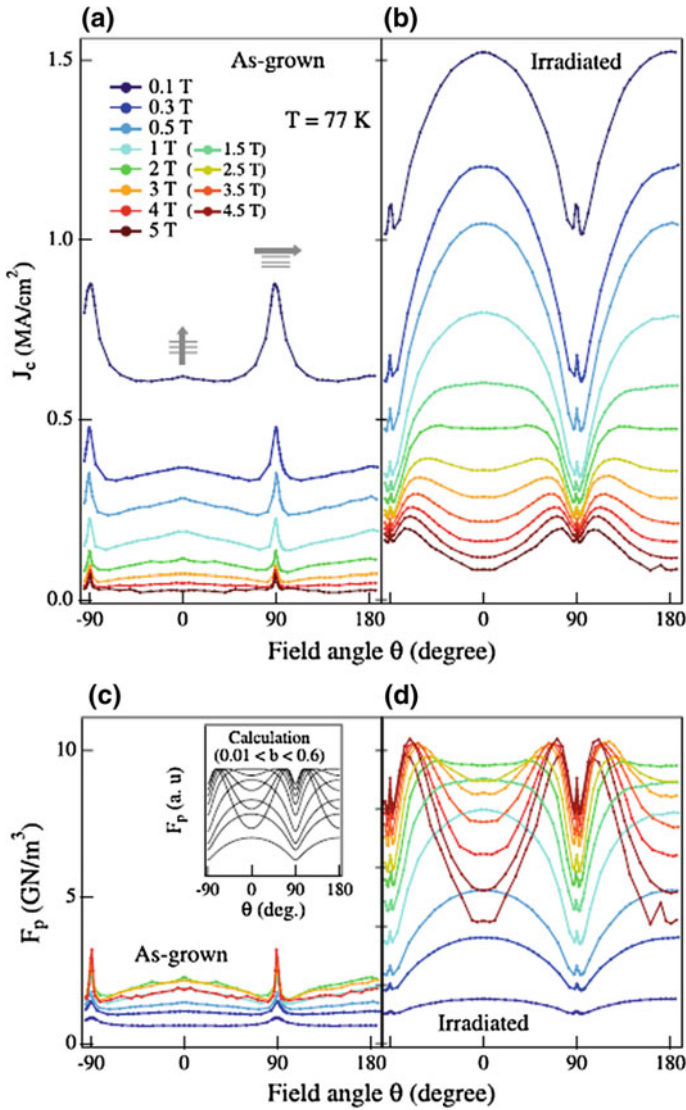
Fig. 4.7 **a** Critical current for as-grown YBCO. **b** J_c for irradiated YBCO, **c** flux pinning force for as-grown YBCO, and inset showing F_p calculation as described in the text, **d** flux pinning force for the irradiated sample. Reprinted from [25] with permission

Fig. 4.7d reasonably well for the field range 2–5 T. This includes fitting the unusual shoulder features which lie at approximately 75°.

Matsui et al. offer the following explanation for their results. The $(m, n) = (0.5, 2)$ values coincide with the predictions of Kramer [26] for point pins, and given the large increase in critical current with the irradiation and hence introduction of point

pins, they naturally ascribe the J_c for B $\geq$ 2 T to strong point pinning. At lower fields, the fitting does not account for a large angle-independent contribution to J_c, and Matsui et al. modify the flux pinning expression with an offset and linear scaling. They justify this with a statistical argument around how pinning may be modified at lower vortex densities.

The $F_p(\epsilon_\theta H)$ scaling observed by Mishev et al. and Matsui et al. is indeed quite striking. We have offered an alternative explanation to the Matsui et al. results in a comment on their paper [27]. Our explanation centers on identifying the equation $f(b) = f_0 b^m (1-b)^n$ as a beta distribution and an outcome of averaging. In both papers, attempts are made to connect the scaling analysis to the microscopic physics. However, in both cases, this raises further questions. For example, in the Matsui et al. data, we may ask why point pinning should lead to the striking shoulder structures.

To make further progress in the next section, we examine direct models which connect the anisotropic critical currents to flux pinning.

4.3 Models of Pinning and Field Angle-Dependent Currents

In view of the open questions about scaling, it is of interest to describe some microscopic models of the critical current anisotropy. Rather than explaining the results through scaling of fundamental equations derived from the Ginsburg-Landau model or the London equations, these are more direct models which seek to link a particular defect structure with the form of $J_c(\theta)$ by considering the forces which are acting on flux lines. We describe the first model in some detail and the following two only briefly.

4.3.1 The Tachiki and Takahashi Model

Tachiki and Takahashi [28] primarily focused on the pinning effect of the layer structure of the superconducting copper oxides. In these materials, the CuO_2 planes are strongly superconductive with a high superfluid density, and the regions between the CuO_2 layers have low superfluid density. The weakly superconducting layers therefore act as natural pinning centers, and when vortices are directed along these layers, they will be strongly pinned against perpendicular motion. Figure 4.8 shows the key idea of their papers. When the magnetic field is at an angle θ, then the vortex forms a staircase structure in which it periodically lies along the *ab*-planes where it is pinned by the intrinsic layers, and intermittently, the vortex is deformed perpendicular to the layers where there is assumed to exist pinning parallel to the *c*-axis through twin planes or other correlated pinning. The twin plane spacing is assumed to be larger than the vortex lattice spacing and the intrinsic layer spacing.
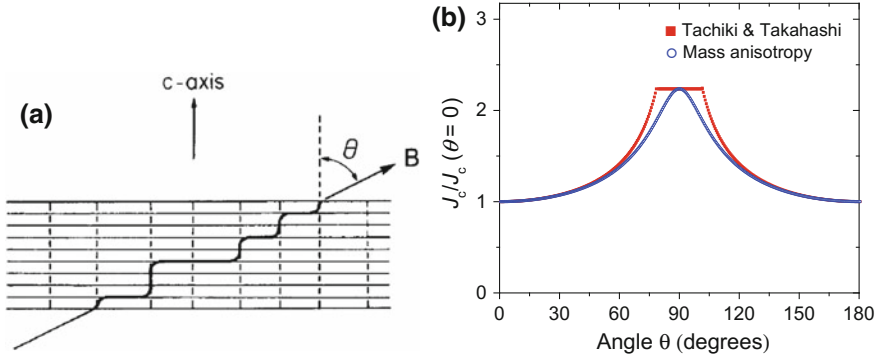
Fig. 4.8 a Vortex at angle θ, being pinned in the *ab*-plane by the intrinsic insulating planes, and pinned in the *c*-axis direction by correlated pinning such as twin planes. (Reproduced by permission from [28]) **b** The angular dependence of critical current according to (4.2), for a sample with $(J_{c\parallel}/J_{c\perp})^2 = 5$, and the mass anisotropy expression with $\gamma = 5$, and in both cases $J_c(B) \propto B^{-0.5}$

The authors then resolve the pinning force into Cartesian components, and derive expressions for J_c when J_c is a result of the Lorentz force exceeding the strength of the layered pinning and then a different expression for when the Lorentz force exceeds the strength of the *c*-axis pinning. Since the flux density from the parallel vortices is $B_x = B\sin\theta$, the critical current is $J_c = J_{c\parallel}(B\sin\theta)$ for the parallel vortices, that is, their pinning forces will be exceeded at this current, where $J_{c\parallel}$ is the critical current in the case of perfect alignment with the *ab*-planes. Tachiki and Takahashi take the parallel field $J_{c\parallel}(B)$ as field independent due to the high matching field for the intrinsic pinning, that is, $J_{c\parallel}(B\sin\theta) = J_{c\parallel}(0)$. The flux density for the *c*-axis oriented vortices is $B_x = B\cos\theta$, and the critical current density for these vortices is $J_c = J_{c\perp}(B\cos\theta)$ when the force parallel to the *c*-axis exceeds the pinning force in this direction. For this direction, they assume a functional dependence $J_{c\perp}(B) \propto B^{-\alpha}$. The overall critical current then depends on which component of pinning force is exceeded, thus

$$J_c(B;\theta) = \min\{J_{c\parallel}(0), J_{c\perp}(B\cos\theta)\} \tag{4.2}$$

Assuming the power law dependence $J_{c\perp}(B) \propto B^{-\alpha}$, we will have at a fixed field $J_c(\theta) \propto (\cos\theta)^{-\alpha}$ for angles not too close to the parallel direction. Tachiki and Takahashi compared (4.2) with data available at the time, and particularly for angles away from parallel field, the fit was reasonably good. The main problem with (4.2) is that it contains an unphysical discontinuity and predicts an angle-independent J_c at parallel field, depending on the ratio of $J_{c\parallel}/J_{c\perp}$, which is not consistent with experiments.

Despite this flaw, this model is instructive and rewards careful consideration. Firstly, it emphasizes that pinned vortices are immobilized in a plane. When they move, it may not be because all pinning forces available are exceeded, but only the

forces necessary to prevent motion in a particular direction. Secondly, (4.2) again returns us to a scaling relation, even though the intention has been to consider pinning forces directly. It can be seen that this scaling relation is effectively the same as the mass anisotropy scaling for field angles near perpendicular. In Fig. 4.8b, we plot (4.2) and the $J_c(\epsilon_\theta B)$ expression assuming we have the power law dependence for the perpendicular field $J_{c\perp}(B) \propto B^{-0.5}$ and $\gamma = 5$. We therefore have reached similar outcomes for the angular dependence over much of the range, although this scaling has been derived solely with reference to correlated pinning.

The assumption that the $J_c(\epsilon_\theta H)$ scaling can uniquely identify isotropic random point pinning is therefore open to question. Note that this identification first made by Civale et al. [15, 16] was never a logical necessity; if random point pins create a scalable dataset, it does not *logically* follow that scaled data imply point pins must be the source.

4.3.2 Models with Anisotropic Vortices

There have been relatively few attempts to construct microscopic models for anisotropic superconductors and point pins. One detailed phenomenological treatment has been made by van der Beek et al. [29]. In their paper, they focus on the multiband iron-based superconductors so that the anisotropy of the coherence length and the penetration depth may be different. They also generalize the isotropic shape of the pins to include ellipsoidal defects. For the single vortex limit, they show that either relatively sharp *ab*-plane peaks or broad *c*-axis peaks can result from the interplay of the anisotropy and the defect size and shape.

The difficulty of constructing microscopic models of pinning was highlighted in a couple of short papers by Mikitik and Brandt [30]. They show how in anisotropic superconductors the force at which vortices move from a pin is not necessarily the same as the pinning force. This is an extension of the idea included in the Tachiki and Takahashi model, where at J_c vortices become unpinned in the direction in the plane where the pinning force is lowest, not the direction of the Lorentz force. Mikitik and Brandt extend this analysis to three dimensions and take account of the fact that anisotropy will create an ellipsoidal pinning force profile in the plane perpendicular to the vortex. Their idea is illustrated in Fig. 4.9. For any pinned vortex, we construct a diagram showing the flux pinning force in any direction in the plane perpendicular to the vortex—$f_p(\Psi)$. If the vortex experiences a force in the direction Ψ, then for a critical force $f_c < f_p(\Psi)$, the vortex will already move in the direction Ψ_1 as the projection of this force at the angle Ψ_1 already exceeds $f_p(\Psi_1)$. We then have to define J_c relative to the critical force f_c not the pinning force f_p.

To construct a microscopic model which can make a credible prediction of the macroscopic $J_c(\theta)$ is hence a daunting task. Reflection on the Tachiki-Takahashi and Mikitik-Brandt models raises a further confounding factor. If we add a particular defect to our pinning landscape and see a significant increase in J_c, then it is
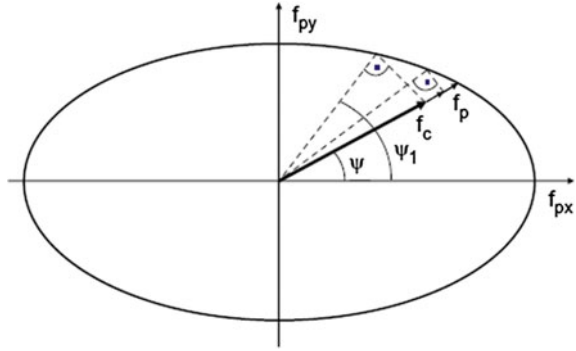
natural to suppose this new defect dominates the pinning. But Tachiki-Takahashi and Mikitik-Brandt show that this is not necessarily the case. The observed $J_c(\theta)$ can be dominated by ineffective pinning in certain directions. Adding pinning which prevents vortex motion in particular directions means that already existing pinning structures may become more effective and relevant in determining $J_c(\theta)$, not less relevant.

Experimentally, the complexity of pinning at the individual vortex level is now being explored through the novel use of scanning probe microscopes [31, 32]. These experiments confirm the complexity of vortex dynamics in response to forces even in quite idealized experimental situations. Another favorable direction for progress is to build computer models based on the Ginzburg–Landau equations which can give a detailed picture of vortex dynamics [33, 34]. At present, the complexity of these models and the computer resources required limit the physical size of the model system. Hence, questions concerning a complex pinning landscape are only just being addressed. A proper summary of these efforts is beyond the scope of this chapter.

In the next section, we will see how the Tachiki-Takahashi model can be extended in a direction which leads us into a different mode of thinking about critical current data, one that has the possibility of making sound inferences for the structure-property relationships.

4.4 The Vortex Path Model or Maximum Entropy Modeling

Rather than the vortex shown in Fig. 4.8a, imagine that the pinning landscape is disordered, and the pinned vortices are more like those of Fig. 4.10. The 'vortex path' through the material as depicted in Fig. 4.10 is a possible state of a pinned vortex which is compatible with an external field at the macroscopic angle θ of this path. The volume pinning strength, and hence J_c, is proportional to the density of such pinning paths through the sample at the angle θ. A function for this density
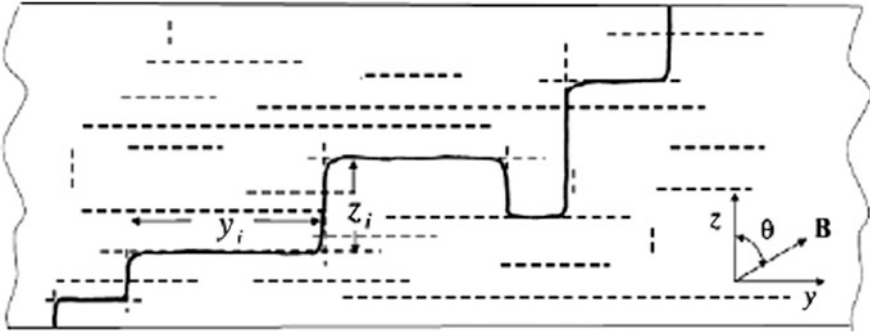
Fig. 4.10 Representation of a vortex pinned both parallel and perpendicular to the *xy* plane and forming a macroscopic angle θ to the *z*-axis. The dotted lines represent pinning defects in the material. This vortex path and others existing in the material can be described as a directed random walk of *n* steps of length y_i in the y-direction and $z_{\text{-}i}$ in the z-direction. An alternative description is to note the defects establish a mean value of *z/y* at which vortices will be pinned, and an associated variance to this mean. Reprinted from [35] with permission

with angle can then be constructed through probabilistic considerations. This leads to a model referred to as the 'vortex path model' [35].

A probability density for the pinning paths, $p(\theta)$, is derived by assuming simple rules for constructing such paths. Consider the vortex path as a directed random walk, where $y = n\lambda$ is the sum of *n* steps of average length λ in the y-direction. This will dictate the center of a peak (though not necessarily a maximum density) in the y-direction. Assuming there is no bias for steps in the z-direction and if the z steps are chosen from any distribution of finite variance, then for $z = \sum_{i=1}^{n} z_i$, the probability for finding a particular *z* value is $p(z) = (1/2\pi n\sigma^2)^{1/2} \exp(-z^2/2n\sigma^2)$, that is, the distribution converges to a Gaussian according to the central limit theorem. As $z/y = \tan\theta$, a transformation of random variables is required to go from $J_c(z/y) \propto p(z)$ to $J_c(\theta) \propto p(\theta)$, with the result

$$J_c(\theta) = \frac{J_0}{\sqrt{2\pi}\Gamma \, \sin^2\theta} \cdot \exp\left(-\frac{1}{2\Gamma^2 \tan^2\theta}\right) \tag{4.5}$$

where $\Gamma = \sigma/\sqrt{n}\lambda$, and J_0 is a proportionality constant. This equation is referred to as an angular Gaussian. If instead of assuming the convergence to a Gaussian for $p(z)$, a heavy tailed Lorentzian distribution is chosen, $p(z) = (1/\pi)\gamma/(\gamma^2 + z^2)$, then the result is

$$J_c(\theta) = \frac{1}{\pi} \frac{J_0 \Gamma}{\cos^2\theta + \Gamma^2 \sin^2\theta} \tag{4.6}$$

where in this case $\Gamma = \gamma/\lambda$, and this is referred to as an angular Lorentzian.

It has been shown [35, 36] that these equations describe $J_c(\theta)$ for an incredibly wide range of samples, for isotropic and anisotropic superconductors. It may however seem that these equations have been derived using contrived rules. After all, are the paths formed by pinned vortices really such a random walk? Won't pinned vortices at large angles from the center angle of such a J_c peak start to follow different rules, dictated by vortex tension, vortex-vortex interactions, or geometric effects of the sample?

Such questions become irrelevant if the distribution in the Cartesian coordinates is taken directly as $p(z/y) = (1/2\pi\,\Gamma^2)^{1/2} \exp(-(z/y)^2/2\Gamma^2)$, that is, a Gaussian in z/y. The model is now independent of the random walk description. A Gaussian is a maximum entropy distribution in which the mean and variance are specified [37]. That is, it is a maximization of the Shannon information entropy with constraints on the mean and variance of the distribution. This is now a maximum entropy model which says the pinning landscape is determining a mean value of z/y at which vortices are pinned in the zy plane (in this case, $<z/y> = 0$), and a variance to this orientation $<(z/y)^2> - <z/y>^2 = \Gamma^2$, but no further information is specified [38]. The angular Lorentzian can likewise be described as a maximum entropy distribution, where only the variance is specified. Any further effect of the physics is 'averaged out,' and we are only left with this information in the data. Maximum entropy can be loosely translated as 'maximum missing information.'

Philosophically, the shift from the vortex path model as describing actual vortex positions, to the maximum entropy description, is a shift from attempting to directly model the microscopic physics, to concentrating on the information content of the $J_c(\theta)$ data. Nonetheless, the vortex configurations described by the vortex path model are a useful physical picture if not taken too literally. The use of maximum entropy distributions to find structure-property relations is the methodology generally employed in spectroscopy, where Gaussian and Lorentzian functions are used, and many other forms of signal processing. Firstly, if the distributions describe the data, then the information content of the data is known with a high degree of confidence. Secondly, the information from the data fitting, in our case the parameters of the $J_c(\theta)$ fitting, can be correlated with information about the microstructure, and hence the structure-property relations of the system determined. We now give some examples from previously published work of applying this process.

Figure 4.11 shows results from Wimbush and Long [36], where a Nb thin film which has an array of vertical pores etched through the film at a spacing of 140 nm and a diameter of 75 nm. The addition of the nanopores increases J_c by up to a factor of 50 over films without nanostructuring. It is known that Nb films will give a strong peak in $J_c(\theta)$ parallel to the plane of the film, so the authors conclude that the vertical pores are contributing to the overall $J_c(\theta)$ but are not creating a peak normal to the film surface. At the lower field, three maximum entropy components are present, a high uniform background, a narrow peak and a broader in-plane peak, both at ±90°. At the higher field, the narrow peak remains similar, but with an even broader peak at 90°, and a broad angular Gaussian at 0°.

Fig. 4.11 $J_c(\theta)$ for a Nb thin film which has been nanostructured with an array of vertical columnar pores: experiment (●), full fit (—), fit components (—,—,—,—). Reprinted by permission from [36]
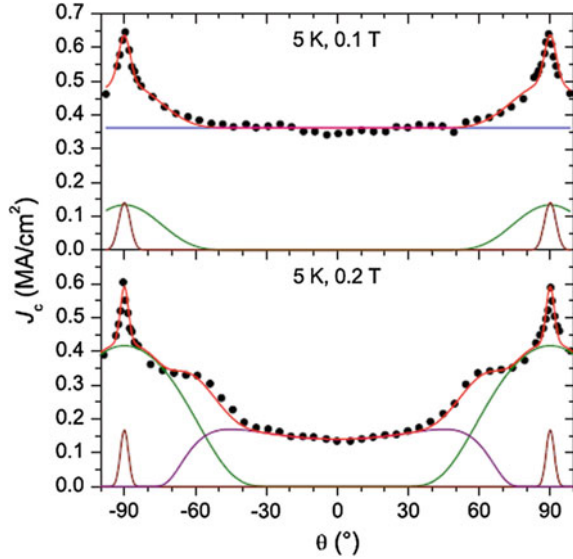
The structure-property relations for the film are then elaborated as follows: The origin of the means at ±90° is the strong in-plane pinning. The mean at 0° at 0.2 T is due to the vertical pores. The origin of the variances is more speculative, but in this system, there are few sources of pinning. The in-plane peaks may be broadened slightly by surface roughness; this is posited as the source of the variance of the narrow peak. Larger broadening of the in-plane peak is achieved by interaction with the pores, that is, there is mixed pinning of the vortices by the in-plane pinning and the pores to broaden these peaks. The angular Gaussian at 0°, 0.2 T, is also a result of mixed pinning, this time with the pores as the dominant contribution and the in-plane pinning as the source of broadening. The constant background at 0.1 T must be due to a dominant contribution from the vertical pores in combination with the in-plane pinning. The field of 0.1 T is approximately the matching field for the pore density, and therefore, the effect of raising the field is to decrease the J_c at 0° relative to the 90° value. The large region of constant $J_c(\theta)$ is easily accommodated in the maximum entropy analysis. In the vortex path model picture, we can think of the pores as fixing the density of possible pinning paths in a way which is angle independent.

The continual search for strategies to increase the critical current of coated conductors is leading to more complex pinning landscapes and resultant complex $J_c(\theta)$ data. The data shown in Fig. 4.12 are from a PLD YBCO sample with $Ba_2YNbO_6 + Gd_3TaO_7$ additions [36]. The resultant microstructure contains c-axis oriented $Ba_2Y(Nb,Ta)O_6$ segmented nanorods, ab-plane oriented Y_2O_3 platelets, and nanoparticles of $YBa_2Cu_4O_8$ superconducting phase.

The maximum entropy fitting in the range of 1–3 T finds there are four components with a mean of 0° (parallel to the c-axis). At 4 T, there is a crossover in
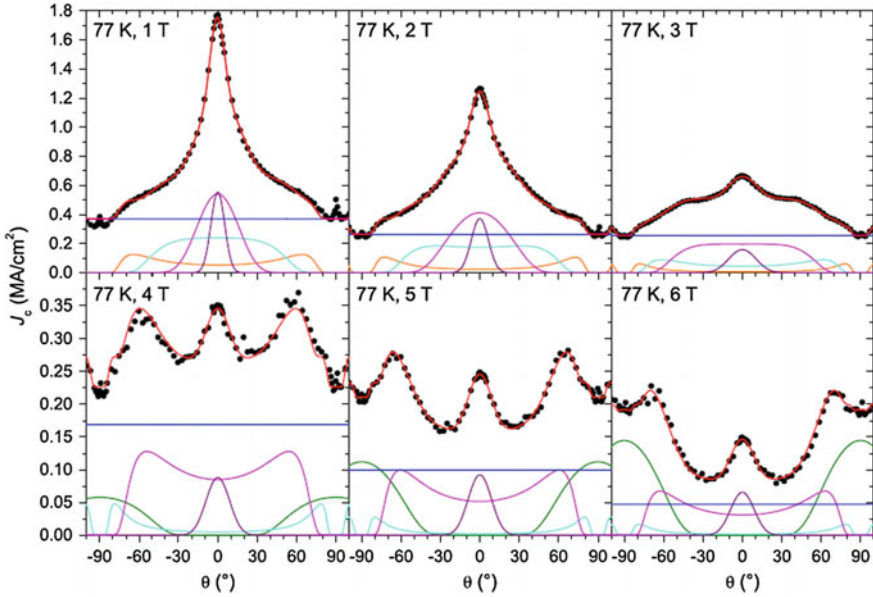
Fig. 4.12 $J_c(\theta)$ for a YBCO film with $Ba_2YNbO_6 + Gd_3TaO_7$ additions. Reprinted by permission from [36]

behavior similar to the Nb sample of Fig. 4.11, and there is a $\pm 90°$ Gaussian peak replacing one of the $0°$ components. The narrowest of these peaks remains relatively unchanged in width for all fields, in comparison with the other $0°$ peaks which become broader. This behavior indicates it has a very high matching field, also the unchanged width indicates the width may arise from the intrinsic angular spread of the defect species itself; hence, this component is identified with the segmented c-axis oriented nanorods. The next broadest of the components has a similar magnitude at all fields but becomes much broader. Hence, it is associated with the same defect species but additionally broadened with interactions with *ab*-planar pinning such as the Y_2O_3 platelets. A description of the origins of other components is given in [36].

The addition of BZO nanoparticles has been a common strategy to increase critical currents in YBCO films. As a final example of the use of vortex path model to find structure-property relations, we show in Fig. 4.13 data from Petrisor et al. [39] who prepared films of YBCO and YBCO + 10 mol% BZO using metal-organic deposition. The results from fitting $J_c(\theta)$ for the undoped and BZO-doped films are shown in Fig. 4.13.

In combination with an analysis of the microstructure, for the pure YBCO, Petrisor et al. assign the narrow *ab* Lorentzian to the intrinsic pinning broadened by lattice disorder including CuO precipitates. The *ab* Gaussian is attributed to the interaction between the intrinsic pinning and the orthogonal pinning by twin planes. The twin planes are also the source of the c-axis Gaussian peak. With the addition

Fig. 4.13 Angle dependence of critical currents for pure YBCO and YBCO +10 mol% BZO at 1 T. Reprinted with permission from [39]
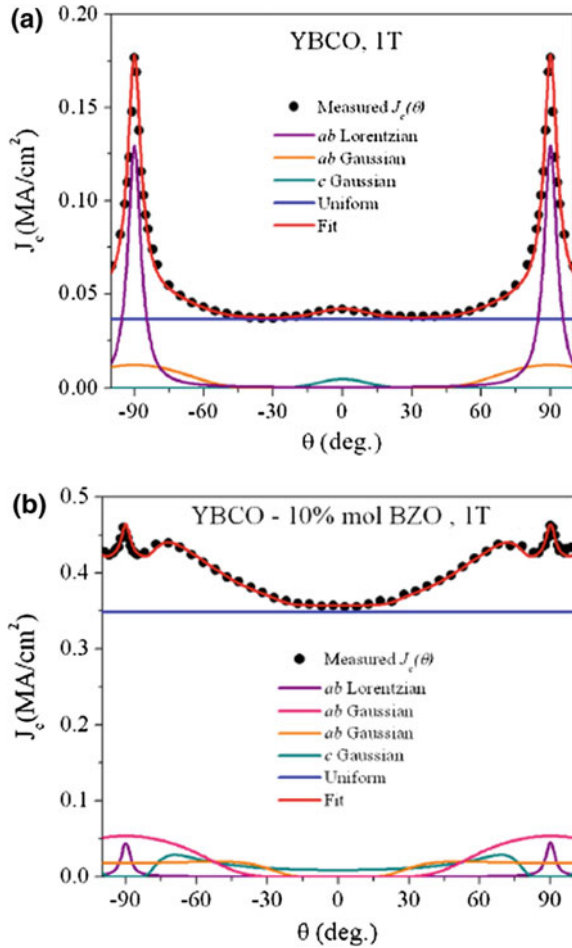
of the BZO, an additional high-intensity *ab* Gaussian peak is observed which they attribute to the additional out of plane straining of the YBCO lattice due to the BZO inclusions which broadens a peak fixed by the intrinsic pinning. The *c*-axis peak under these conditions becomes extremely broadened by interaction with the intrinsic *ab*-plane pinning giving rise to the shoulders around $\pm 70°$. The additional strain of the BZO inclusions also gives rise to the very high isotropic component of the J_c, consistent with the results of Llordés et al. [18].

Other groups who have shown the usefulness of the vortex path model include the University of Turku group [40–42] who have used it to compare theoretical and measured values of the peak widths of YBCO films [40]. They also introduced using the pseudo-Voigt function which is a linear combination of (4.5) and (4.6) to get a better fit of peak shapes. In [41], they showed how the method can determine the contribution of *c*-axis aligned defects, even when a *c*-axis peak is not visible in

the data. This group uses an explicit elliptical term in their fitting to account for the effect of mass anisotropy on point defect pinning. We do not believe this is necessary and would only consider adding this term if (4.5) and (4.6) could not account for the data without modification.

Other noteworthy publications showing the ability of the vortex path model to accurately fit data include Hänisch et al. [43] for iron arsenide superconductor films, Mikheenko et al. [44] for YBCO with BZO nanocolumns, and Talantsev et al. [45] used it to show a correlation between stacking fault density and *ab*-peak height, showing the dominance of this defect at low fields and high temperatures in MOD YBCO films.

4.5 Conclusions

Although a large literature exists of experimental data and a smaller literature of relevant models, a satisfactory consensus does not yet exist on understanding the structure-property relations of $J_c(\theta)$ data, and by extension critical currents generally. There is a consensus that samples in the regime of weak collective pinning from point pins should obey $J_c(\epsilon_\theta H)$ scaling. This behavior has been observed consistent with the mass anisotropy of the material. A $J_c(\epsilon_\theta H)$ scaling behavior has also been shown for BSCCO and YBCO samples, where scaling parameters are not consistent with the known electronic mass anisotropy. The origins of this scaling are not clear, but such behavior can arise through pinning from correlated defects, and it is not unreasonable to believe it can come from some kind of averaging over both correlated and uncorrelated pinning.

Intriguingly, $F_p(\epsilon_\theta H)$ scaling has also been observed for samples with added isotropic pinning centers. It has been proposed that this arises due to pinning from defects larger than the coherence lengths, although the microscopic explanation of this is not really convincing. It will be interesting to observe in the near future how common this form of scaling is for samples with high levels of defect engineering.

There are few microscopic models which aid our understanding of $J_c(\theta)$. This is perhaps not surprising as there are serious obstacles to constructing such models, particularly once mixed pinning is introduced. To accurately model pinning, vortices need to be treated as three-dimensional objects moving in three-dimensional space. We have presented the model of Tachiki and Takahashi and the key ideas of Mikitik and Brandt as giving worthwhile insight into the difficulties.

The vortex path model or maximum entropy modeling provides an alternative approach which avoids the difficulties of constructing or relying on the results from microscopic models. It is a statistical-based approach similar to conventional spectroscopy analysis which begins with determining the information content of the data. Combined with microstructural analysis, this approach can be used to build up knowledge of structure-property relations with a high degree of confidence.

References

1. J.L. MacManus-Driscoll et al., Strongly enhanced current densities in superconducting coated conductors of $YBa_2Cu_3O_{7-x}$ + $BaZrO_3$. Nat. Mater. **3**, 439 (2004)
2. J. Gutiérrez et al., Strong isotropic flux pinning in solution-derived $YBa_2Cu_3O_{7-x}$ nanocomposite superconductor films. Nat. Mater. **6**, 367 (2007)
3. V. Selvamanickam et al., High critical currents in heavily doped (Gd, Y) Ba_2Cu_3Ox superconductor tapes. Appl. Phys. Lett. **106**, 032601 (2015)
4. M. Miura et al., Mixed pinning landscape in nanoparticle-introduced $YGdBa_2Cu_3Oy$ films grown by metal organic deposition. Phys. Rev. B **83**, 184519 (2011)
5. S.R. Foltyn et al., Materials science challenges for high-temperature superconducting wire. Nat. Mater. **6**, 631 (2007)
6. A. Goyal et al., Irradiation free, columnar defects comprised of self-assmbled nanodots and nanorods resulting in strongly enhanced flux pinning in $YBa_2Cu_3O_7$-d films. Supercond. Sci. Technol. **18**, 1533 (2005)
7. M. Igarashi et al., Advanced development of IBAD/PLD coated conductors at FUJIKURA. Phys. Procedia **36**, 1412–1416 (2012)
8. G. Blatter, M. V. Feigel'man, V.B. Geshkenbein, A.I. Larkin, V.M. Vinokur, Vortices in high-temperature superconductors. Rev. Mod. Phys. **66**, 1125 (1994)
9. D.-X. Chen, J.J. Moreno, A. Hernando A. Sanchez, B.-Z. Li, Nature of the driving force on an Abrikosov vortex. Phys Rev. B. **57**, 5059 (1998)
10. J. Castro, A. Lopez, Comments on the force on pinned vortices in superconductors. J. Low Temp. Phys. **135**, 15 (2004)
11. G. Blatter, V.B. Geshkenbein, A.I. Larkin, From isotropic to anisotropic superconductors: a scaling approach. Phys. Rev. Lett. **68**, 875–878 (1992)
12. Z. Hao, J.R. Clem, Angular dependencies of the thermodynamic and electromagnetic properties of the high—Tc superconductors in the mixed state. Phys. Rev. B. **46**, 4833–5856 (1992)
13. X. Xu, J. Fang, X. Cao, K. Li, W. Yao, Z. Qi, Angular dependence of the critical current density for epitaxial $YBa_2Cu_3O_7$-d thin film. Solid State Commun. **92**, 501–504 (1994). X. Xu, J. Fang, X.W. Cao and K Li, A scaling formula of critical current density for anisotropic superconductors. J. Phys D: Appl. Phys. **29**, 2473 (1996)
14. G.R. Kumar, M.R. Koblischka, J.C. Martinez, R. Griessen, B. Dam, J. Rector, Angular scaling of critical current measurements on laser-ablated $YBa_2Cu_3O_7$−d thin films. Physica C **235–240**, 3053 (1994)
15. L. Civale et al., Understanding high critical currents in YBa2Cu3O7 thin films and coated conductors. J. Low. Temp. Phys. **135**, 87 (2004)
16. L. Civale et al., Angular-dependent vortex pinning mechanisms in $YBa_2Cu_3O_7$ coated conductors and thin films. Appl. Phys. Lett. **84**, 2121 (2004)
17. J. Gutiérrez et al., Anisotropic c-axis pinning in interfacial self-assembled nanostructured trifluoroacetate-$YBa_2Cu_3O_7$-x films. Appl. Phys. Lett. **94**, 172513 (2009)
18. A. Llordés et al., Nanoscale strain-induced pair suppression as a vortex-pinning mechanism in high-temperature superconductors. Nat. Mater. **11**, 329 (2012)
19. S.C. Wimbush, N.M. Strickland, N.J. Long, Low-Temperature scaling of the critical current in 1G HTS wires. IEEE Trans. Appl. Supercond. **25**, 6400105 (2015)
20. G. Grasso, Processing of high Tc conductors: the compound B,Pb(2223), in *Handbook of Superconducting Materials* v1, ed. by D.A. Cardwell, D.S. Ginley (IoP Publishing, Bristol and Philadelphia, 2003)
21. N. Clayton, N. Musolino, E. Giannini, V. Garnier, R. Flükiger, Growth and superconducting properties of $Bi_2Sr_2Ca_2Cu_3O_{10}$ single crystals. Supercond. Sci. Technol. **17**, S563–S567 (2004)
22. D.K. Hilton, A.V. Gavrilin, U.P. Trociewitz, Practical fit functions for transport critical current versus field magnitude and angle data from (RE)BCO coated conductors at fixed low temperatures and in high magnetic fields. Supercond. Sci. Technol. **28**, 074002 (2015)

23. E. Pardo, M. Vojenciak, F. Gomory, J. Souc, Low-magnetic-field dependence and anisotropy of the critical current density in coated conductors. Supercond. Sci. Technol. **24**, 065007 (2011)
24. V. Mishev et al., Interaction of vortices in anisotropic superconductors with isotropic defects. Supercond. Sci. Technol. **28**, 102001 (2015)
25. H. Matsui et al., Dimpling in critical current density versus magnetic field angle in $YBa_2Cu_3O_7$ films irradiated with 3-MeV gold ions. J. Appl. Phys. **114**, 233911 (2013)
26. E.J. Kramer, Scaling laws for flux pinning in hard superconductors. J. Appl. Phys. **44**, 1360 (1973)
27. N.J. Long, S.C. Wimbush, Comment on Dimpling in critical current density versus magnetic field angle in $YBa_2Cu_3O_7$ films irradiated with 3-MeV gold ions [J. Appl. Phys. **114**, 233911 (2013)]. J. Appl. Phys. **115**, 136101 (2014)
28. M. Tachiki, S. Takahashi, Anisotropy of critical current in layered oxide superconductors. Solid State Commun **72**, 1083–6 (1989). M. Tachiki and S. Takahashi, "Intrinsic pinning in cuprate superconductors. Appl. Supercond. **2**, 305–313 (1994)
29. C.J. van der Beek, M. Konczykowski, R. Prozorov, Anisotropy of strong pinning in multi-band superconductors. Supercond. Sci. Technol. **25**, 084010 (2012)
30. G.P. Mikitik, E.H. Brandt, Flux-line pinning by point defects in anisotropic biaxial type-II superconductors. Phys. Rev. B **79**, 020506(R) (2009). Flux-line pinning by point defects in anisotropic type-II superconductors. Physica C **470**, S892–S893 (2010)
31. L. Embon et al., Probing dynamics and pinning of single vortices in superconductors at nanometer scales. Sci Rep. **5**, 7598 (2015)
32. O.M. Auslaender et al., Mechanics of individual isolated vortices in a cuprate superconductor. Nat. Phys. **5**, 35 (2009)
33. Q. Du, Numerical approximations of the Ginzburg-Landau models for superconductivity. J. Math. Phys. **46**, 095109 (2005)
34. I.A. Sadovskyy, A.E. Koshelev, C.L. Phillips, D.A. Karpeyev, A. Glatza, Stable large-scale solver for Ginzburg-Landau equations for superconductors. J. Comput. Phys. **294**, 639 (2015)
35. N.J. Long, Model for the angular dependence of critical currents in technical superconductors. Supercond. Sci. Technol. **21**, 025007 (2008)
36. S.C. Wimbush, N.J. Long, The interpretation of the field angle dependence of the critical current in defect-engineered superconductors. New J. Phys. **14**, 083017 (2012)
37. J.N. Kapur, *Maximum-Entropy Models in Science and Engineering*, 2nd edn. (New Age, New Delhi, India, 2009)
38. N.J. Long, Maximum entropy distributions describing critical currents in superconductors. Entropy **15**, 2585 (2013)
39. T. Petrisor et al., The vortex path model analysis of the field angle dependence of the critical current density in nanocomposite YBa_2Cu3O_{7-x}-$BaZrO_3$ films obtained by low fluorine chemical solution deposition. J Supercond. Nov. Magn. **27**, 2493–2500 (2014)
40. P. Paturi, The vortex path model and angular dependence of Jc in thin YBCO films deposited from undoped and $BaZrO_3$ doped targets. Supercond. Sci. Technol. **23**, 025030 (2010)
41. M. Malmivirta et al., Three ranges of the angular dependence of critical current of $BaZrO_3$ doped $YBa_2Cu_3O_{7-d}$ thin films grown at different temperatures. Thin Solid Films **562**, 554–560 (2014)
42. M. Malmivirta et al., The angular dependence of the critical current of baCeO3 doped $YBa_2Cu_3O_6$+x thin films. IEEE Trans. Appl. Supercond. **25**, 6603305 (2015)
43. J. Hänisch, K. Iida, F. Kurth, T. Thersleff, S. Trommler, E. Reich, R. Hühne, L. Schultz, B. Holzapfel, the effect of 45° grain boundaries and associated Fe particles on Jc and resistivity in Ba(Fe 0.9Co 0.1)2As2 thin films. Adv. Cryogenic Eng. **1574**, 260 (2014)
44. P. Mikheenko et al., Integrated nanotechnology of pinning centers in $YBa_2Cu_3O_x$ films. Supercond. Sci. Technol. **23**, 125007 (2010)
45. E.F. Talantsev et al., Hole doping dependence of critical current density in $YBa_2Cu_3O_7$ conductors. Appl. Phys. Lett. **104**, 242601 (2014)